Solar Energy Materials & Solar Cells 142 (2015) 123–127

Contents lists available at ScienceDirect

Solar Energy Materials & Solar Cells

journal homepage: www.elsevier.com/locate/solmat

# Tunnel oxide passivated carrier-selective contacts based on ultra-thin $SiO_2$ layers

Anamaria Moldovan*, Frank Feldmann, Martin Zimmer, Jochen Rentsch, Jan Benick, Martin Hermle

*Fraunhofer Institute for Solar Energy Systems (ISE), Heidenhofstraße 2, 79110 Freiburg, Germany*

ARTICLE INFO

*Article history:*
Received 6 April 2015
Received in revised form
22 June 2015
Accepted 25 June 2015
Available online 8 July 2015

*Keywords:*
Passivated contacts
Carrier-selective contacts
Tunnel oxide
Interface structure
XPS
TEM

ABSTRACT

Carrier-selective contacts are one of the key enabling technologies to approach very high conversion efficiencies close to the theoretical limit of silicon solar cells. The tunnel oxide passivated contact (TOPCon) approach is an alternative to classical heterojunction solar cells enabling efficiencies up to 24.4%. The tunnel oxide is a core element of this contact as it has to reduce the minority carrier recombination but simultaneously must not hamper the majority carrier flow. This paper focuses on ozone-based oxidation techniques, which can potentially be cost effective and industrially feasible methods for the realization of ultra-thin tunnel oxide layers as an alternative to the oxidation in nitric acid ($HNO_3$) reference process. All investigated oxides were applied to the electron-selective contact (n-TOPCon) on planar and textured surfaces. It will be shown that both ozone based oxidation techniques ($UV/O_3$ photo-oxidation and wet-chemical oxidation in ozonized DI-$H_2O$) enable high implied open circuit voltage ($iV_{OC}$) values exceeding 720 mV on planar and 710 mV on textured surfaces, respectively. Further oxide properties as stoichiometry and layer thickness were analyzed by means of X-ray photoelectron spectroscopy (XPS), spectral ellipsometry (SE) and transmission electron microscopy (TEM). In compliance with earlier results it was found that a minimum oxide layer thickness (approximately 1.3 nm) and a high amount of oxygen-rich sub oxide species are required to obtain a good surface passivation. Using such oxides, a wider range of temperatures can be used during the TOPCon annealing. Applying the ozone-based oxide layers to n-TOPCon solar cells resulted in a high $V_{OC}$ of up to 719 mV and a peak efficiency of 24.9%. Similar results were obtained with the $HNO_3$ reference process ($V_{OC}$=716 mV, $\eta$=24.8%).



## 1. Introduction

The tunnel oxide passivated contact (TOPCon) [1] consists of a stack of an ultra-thin tunnel oxide layer and a doped Si layer which partially crystallizes upon annealing. In the case of the phosphorus-doped electron-selective contact (n-TOPCon) an excellent surface passivation was achieved ($J_{0,rear} < 10$ fA/cm$^2$). Replacing the point contact scheme of an n-type Si PERL solar cell with B-diffused emitter, the passivated contact enabled a high $V_{OC}$ of 715 mV and very high *FF* of 82.1% due to its excellent carrier-selectivity and its one dimensional carrier flow pattern in the base. Altogether with an optimized front side a conversion efficiency of 24.4% was demonstrated [2].

Since the quality of the tunnel oxide is crucial for the surface passivation the main purpose of this publication is to draw a comparison between the standard wet-chemical $HNO_3$ oxide, a dry-grown $UV/O_3$ oxide [3], and a wet-chemical oxide grown in ozonized DI-$H_2O$ ($DIO_3$). The different oxidation technologies are compared using microstructural analysis but also at device level.

Beside the potentially lower process costs for the ozone based oxide, it was already shown that $UV/O_3$ grown oxides allow for higher thermal annealing temperatures which can be attributed to a favorable interface stoichiometry of the grown oxide [3]. As described in literature [4–7] ozone-grown oxides are found to exhibit improved interface (less strain, transition layer is reduced, high density and less defects due to more saturated Si–O bonds) and electrical properties due to the occurring damage-free oxidation of the silicon surface. In addition, it is assumed that atomic oxygen is the main driving force of the oxidation because it is the species that has the feature to be particularly diffusion active in the $SiO_x$ layer and saturate silicon dangling bonds [8]. The resulting oxide layers are supposed to have a higher density (2.11 g/cm$^3$ for $HNO_3$ vs. 2.20–2.24 g/cm$^3$ for thermal oxide vs. 2.21–2.25 g/cm$^3$ for

* Corresponding author. Tel.: +49 761 4588 5536.
*E-mail address:* anamaria.moldovan@ise.fraunhofer.de (A. Moldovan).

http://dx.doi.org/10.1016/j.solmat.2015.06.048
0927-0248/

$O_3$ based oxides [7]), have a lower amount of defects [7] and their structure is closer to that of stoichiometric $SiO_2$ [3].

## 2. Experimental

### 2.1. Sample preparation

Symmetrical lifetime samples were realized on planar (shiny-etched) and alkaline textured n-type 1 Ω cm (100) – oriented FZ silicon wafers with a thickness of 200 μm. The wafers were wet chemically cleaned according to the RCA procedure [9]. The tunnel oxide layer having an approximate thickness of 1.3–1.5 nm was either wet chemically grown in 68 wt% nitric acid at 110 °C for 10 min [10,11] or in ozonized DI-water with a constant ozone concentration of 30 ppm at 30 °C and varying exposure time ($t$=3, 5, 10 and 15 min). Alternatively the oxide layer was generated by photo-oxidation with an UV excimer source [3,12]. The UV excimer source emits monochromatic UV light at a wavelength of 172 nm which dissociates molecular oxygen ($O_2$) of the ambient atmosphere. The resulting atomic oxygen can then directly react with the silicon surface or with $O_2$ to form ozone ($O_3$) which is also a highly oxidizing species and interacts fast with the silicon surface. The oxide growth was influenced by varying the distance between wafer and source ($d$=0.2, 0.5, 1.5 cm) as well as the exposure time ($t$=1, 3, 5 min) [3]. Subsequently, a 15 nm thin phosphorus (P)-doped silicon layer was deposited on both sides. Upon deposition, the samples were annealed within a tube furnace process at the two distinctive temperatures 800 °C and 900 °C. The amorphous structure of the doped Si layer can be entirely sustained with only negligible dopant diffusion into the c-Si at 800 °C. On the other hand, the 900 °C anneal leads to a partial crystallization of the Si layer and a shallow diffusion into c-Si. The partial crystallization of the Si film is also beneficial in terms of mitigating parasitic absorption when TOPCon is placed on the front side [13]. The samples then received a 30-min anneal at 400 °C in an atomic hydrogen atmosphere (Remote Plasma Hydrogen Passivation (RPHP)) [14]. The injection-dependent carrier lifetime characteristics were measured by the quasi-steady-state photo-conductance (QSSPC) technique. These curves were then translated into implied $J$–$V$ curves which yielded the $iV_{oc}$ at 1 sun and the implied fill factor ($iFF$) [15].

### 2.2. Characterization of tunnel-oxide layer

The thickness of the $SiO_x$ layers was experimentally determined by spectral ellipsometry (SE) using a model for native oxide to allow for a qualitative comparison. Both, the wet-chemical oxidation in $HNO_3$ or $DIO_3$ and the UV/$O_3$ oxidation are self-limiting processes. Using UV/$O_3$ oxidation, the oxide growth saturated after about 3 min exposure time and a final oxide thickness of 14–15 Å was determined by SE (see Fig. 1). In comparison the $HNO_3$ oxide turned out to be of similar thickness (about 14 Å) (see Fig. 1). The obtained $SiO_x$ layer thicknesses are in agreement with data resulting from TEM analysis (approximately 13 Å) (see Fig. 2). However, the values resulting from the SE measurement are supposed to be overestimated to some extent due to inaccuracies regarding the applied model for the data interpretation. For the wet-chemical oxidation in ozonized DI-$H_2O$ comparable oxide thicknesses in the range of 13 Å were obtained after 10–15 min whereby for shorter exposure times the oxide growth was not completed and a thickness of 11–12 Å was reached (see Fig. 1).

In a next step the oxides were analyzed by X-ray photoelectron spectroscopy (XPS). The main results obtained from an investigation reported in Ref. [3] were that there are structural differences concerning the stoichiometry of $HNO_3$ and UV/$O_3$ grown oxides

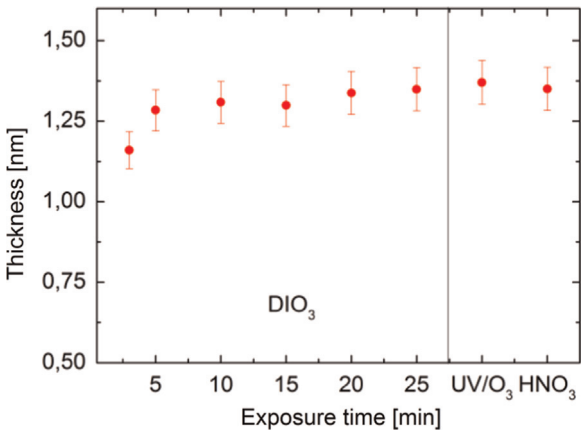


**Fig. 1.** Layer thickness plotted against exposure time for $DIO_3$ oxides and for the UV/$O_3$ (3 min exposure time, 0.5 cm distance to irradiation source) and $HNO_3$ reference process (10 min exposure time).

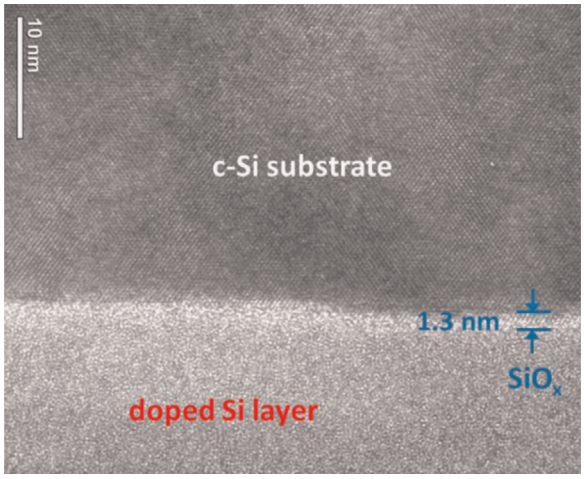


**Fig. 2.** TEM cross-section of ultra-thin oxide layer prepared by UV/$O_3$ oxidation (3 min exposure time, 0.5 cm distance to irradiation source).

and that a longer exposure time and/or a reduced distance lead to more stoichiometric oxides for the UV/$O_3$ oxides [3].

Similar tendencies are observed within the XPS analysis of the $DIO_3$ oxide layers in dependence of the exposure time. The "suboxide-ratio" which is defined in this paper as the ratio between the Si-rich ($Si^{+1}$) and the O-rich ($Si^{2+}$, $Si^{3+}$) suboxide species decreases with an extended exposure time and indicates that a higher amount of oxygen-rich Si-suboxides is present in the oxide layer. The comparison of the UV/$O_3$ (3 min exposure time, 0.5 cm distance to irradiation source) and the newly investigated wet-chemically grown $DIO_3$ oxides shows a comparable thickness and stoichiometric composition (higher amount of oxygen-rich Si-suboxides (expressed in the "suboxide-ratio") after an exposure of approximately 15–25 min (Table 1).

In contrast the $HNO_3$ oxide of approximately the same thickness has a significant higher "suboxide-ratio" and therefore a lower amount of oxygen-rich Si-suboxides (Table 1). In summary, the obtained results indicate that the composition of the non-stoichiometric $SiO_x$ layer is dependent on the oxidation mechanism and the kinetics of the occurring reactions [16].

### 2.3. Surface passivation

The surface passivation quality of these different oxides was tested on symmetrical lifetime samples. Fig. 3 depicts the implied $V_{oc}$ values achieved with the $DIO_3$ oxides (for $O_3$ concentration of

**Table 1**
Percentage of the $Si^{1+}$, $Si^{2+}$ and $Si^{3+}$ peaks obtained from XPS analysis, calculated "suboxide-ration" and oxide layer thickness determined by SE and TEM if available. The data points marked with n.a. are not available within this analysis.

| Oxide | $Si^{1+}$ | $Si^{2+}$ | $Si^{3+}$ | $Si^{1+}/Si^{2+}+Si^{3+}$ | SE Oxide thickness [nm] | TEM Oxide thickness [nm] |
|---|---|---|---|---|---|---|
| $DIO_3$ (30 ppm, 3 min) | n.a. | n.a. | n.a. | n.a. | 1.2 | n.a. |
| $DIO_3$ (30 ppm, 5 min) | 4.53 | 0.52 | 0.30 | 5.52 | 1.3 | n.a. |
| $DIO_3$ (30 ppm, 10 min) | 3.85 | 0.46 | 0.31 | 5.00 | 1.3 | n.a. |
| $DIO_3$ (30 ppm, 15 min) | 3.97 | 0.51 | 0.33 | 4.73 | 1.3 | n.a. |
| $DIO_3$ (30 ppm, 25 min) | 4.14 | 0.57 | 0.35 | 4.50 | 1.4 | n.a. |
| $UV/O_3$ (0.5 cm, 3 min) | 3.77 | 0.49 | 0.39 | 4.28 | 1.4 | 1.1–1.3 |
| $HNO_3$ Ref. | 4.17 | 0.17 | 0.27 | 9.48 | 1.4 | 1.1–1.3 |

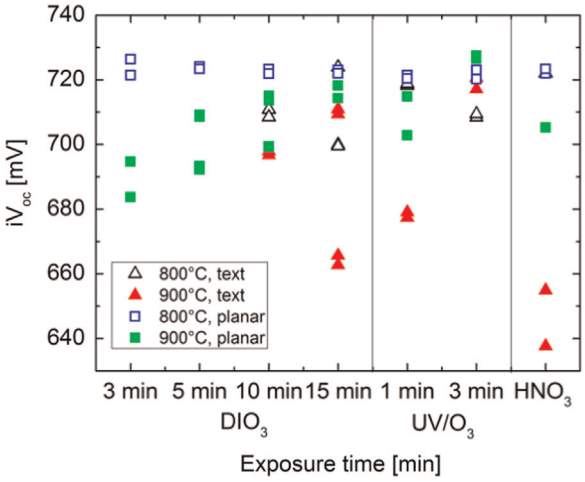


**Fig. 3.** $iV_{OC}$ data of symmetrical lifetime samples of the TOPCon n-contact for the 3 investigated oxidation processes for different exposure times.

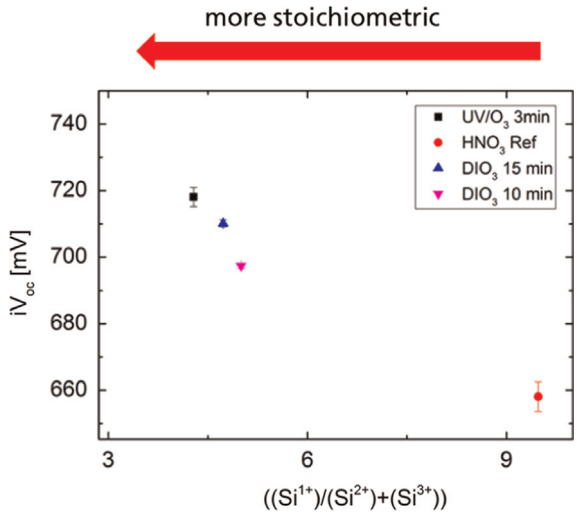


**Fig. 4.** $iV_{OC}$ (textured samples, annealed at $T=900\,°C$) plotted against the "sub-oxide-ratio", comparison of $HNO_3$, $UV/O_3$ and $DIO_3$ oxide layers.

30 ppm and exposure times of 3, 5, 10 and 15 min) and those of the $UV/O_3$ (0.5 cm distance to irradiation source, 1 and 3 min exposure time) and $HNO_3$ oxides as a reference. For an annealing at 800 °C (closed symbols) each oxide yielded a good surface passivation characterized by an $iV_{oc} > 715$ mV on planar and an $iV_{oc} > 700$ mV on textured surfaces. For both, $UV/O_3$ and wet-chemically grown $O_3$ oxide, a longer oxidation time is required to get a good passivation quality for the samples annealed at 900 °C (open symbols). Especially on textured surfaces (triangular symbols) and for 900 °C annealing, the $O_3$ based oxides ($iV_{oc}$=705–720 mV) outperform the $HNO_3$ oxide ($iV_{oc}$=635 mV). Compared to $UV/O_3$, the $DIO_3$ oxidation process seems to be more sensitive since partially a significant variation of the $iV_{OC}$ values can be observed.

### 2.4. Impact of stoichiometry on $iV_{OC}$

For the quantification of the passivation quality in dependence of the stoichiometry the "suboxide-ratio" is set in correlation with the $iV_{OC}$ values obtained at an annealing temperature of 900 °C for samples with a textured surface (see Fig. 4). It can be assumed that oxide layers with a more stoichiometric structure provide a better passivation quality and result in a higher $iV_{OC}$.

$UV/O_3$ oxide layers are supposed to be less prone to disruption at higher annealing temperatures. This can be attributed to their structural composition which includes more O-saturated Si-bonds and results from the fast kinetics of the oxidation and diffusion reaction. In addition, a high amount of reactive oxygen species (atomic oxygen and ozone) is available for the reaction due to the high energy input of the excimer radiation source. The reaction mechanism of the $DIO_3$ oxidation proceeds in a comparable manner as the $UV/O_3$ oxidation (as the same reactive oxygen species are available). However, the kinetics of the reaction is slower in aqueous solution, so that extended exposure times are required to produce oxide layers with a more stoichiometric structure comparable to that of the $UV/O_3$ oxide (see Fig. 4). For an extended exposure time the "suboxide-ratio" of the $DIO_3$ oxide layer decreases (as a higher amount of more stoichiometric species is present in the oxide layer) and the $iV_{OC}$ value increases.

In comparison to the $O_3$-based oxidation the reaction in $HNO_3$ is much slower if not carried out at elevated temperatures as $HNO_3$ first has to decompose to provide reactive oxygen species.

$$2HNO_3 \rightarrow NO_2 + NO + H_2O + 2O \quad (2.1)$$

It can be assumed that due to the slower oxidation reaction more defects in sub-stoichiometric interface layer are present when the oxidation of the first monolayers is accomplished. Furthermore, less diffusion through the stoichiometric amorphous $SiO_2$ layer that grows on top of the sub-stoichiometric interface layer is possible to saturate Si-dangling bonds.

### 2.5. Nanostructure analysis of the Si–$SiO_2$ interface

TEM cross sections of the textured $iV_{OC}$ samples with $HNO_3$ and $UV/O_3$ oxide annealed at 900 °C were fabricated to verify if the decreased $iV_{OC}$ value of the $HNO_3$ oxide sample can be attributed to disruptions of the $SiO_x$ layer. As depicted in Fig. 5a the $HNO_3$ oxide layer is inhomogeneous and partially disrupted whereas the $UV/O_3$ oxide layer (Fig. 5b) is homogeneous and continuous. Hence, the recent findings give further evidence for the hypothesis that the stability of the passivation is dependent on the stoichiometry of the interfacial $SiO_x$ layer.

### 2.6. TOPCon solar cells

To investigate whether the ozone based oxide layers ($UV/O_3$ and $DIO_3$) are also applicable on cell level, solar cells with a diffused boron-doped emitter at the front side and n-TOPCon at the rear side were fabricated. The cells featuring a boron front emitter were processed on n-type 1 Ω cm FZ silicon wafers with a thickness of 200 μm. In addition to the optimized tunnel oxide formation other features to improve the cell efficiency were implemented. More details can be found in an upcoming publication [17].

The cells with the $HNO_3$ reference tunnel oxide layer were annealed at 800 °C. The cells with the ozone based tunnel oxide layers ($UV/O_3$ and $DIO_3$) were annealed at 800 °C and 900 °C. In general $V_{OC}$ for all considered processes is high, resulted in a $V_{OC}$ of up to 719 mV (see Fig. 6a). The slightly lower values of the $UV/O_3$ oxide ($T_{anneal}$=800 °C) are assumed to arise as a result of process variations.

Nearly the same high efficiencies were reached for all three oxidation processes, however for different annealing conditions: $T_{anneal}$=800 °C for the $HNO_3$ reference process and $T_{anneal}$=900 °C for the ozone-based $UV/O_3$ and $DIO_3$ oxidation. The cells with $UV/O_3$ and $DIO_3$ tunnel oxide layer annealed at 800 °C have a lower efficiency value which is mainly due to a lower *FF*. The main drop in *FF* can be associated with a lower passivation quality at low injection conditions and manifests itself in a lower *pFF* of about 82–83%.

A peak efficiency of 24.9% ($V_{OC}$=719 mV) could be obtained for a cell featuring an $UV/O_3$ oxide layer ($T_{anneal}$=900 °C). Similar results were obtained with the $HNO_3$ reference process ($V_{OC}$=716 mV, $\eta$=24.8%). The solar cell results (of the champion cells of the $UV/O_3$ and $HNO_3$ group) were independently confirmed by Fraunhofer ISE Callab.

## 3. Summary and conclusion

Alternative cost effective and for the industrial production feasible methods to grow the tunnel oxide layer for TOPCon based on ozone were presented: $DIO_3$ and $UV/O_3$. The oxides' stoichiometry and thicknesses were evaluated and compared to the $HNO_3$ reference. It was found that the oxidation in $DIO_3$ can result into thermally more stable oxides which also enabled an improved surface passivation quality for n-TOPCon on textured surfaces even though the full $iV_{oc}$ potential achieved with the $UV/O_3$ has not been reached yet. A detailed analysis concerning oxide properties and possible inter-relations between these and the stability of

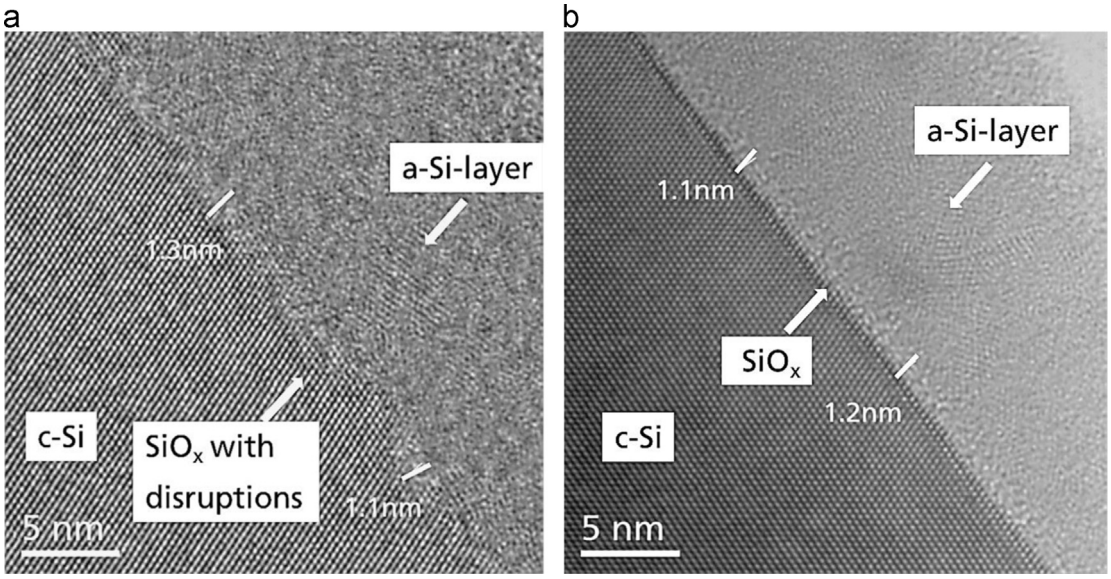


**Fig. 5.** (a) Cross section of $iV_{OC}$ sample with $HNO_3$ oxide annealed at 900 °C. (b) Cross section of $iV_{OC}$ sample with $UV/O_3$ oxide annealed at 900 °C.

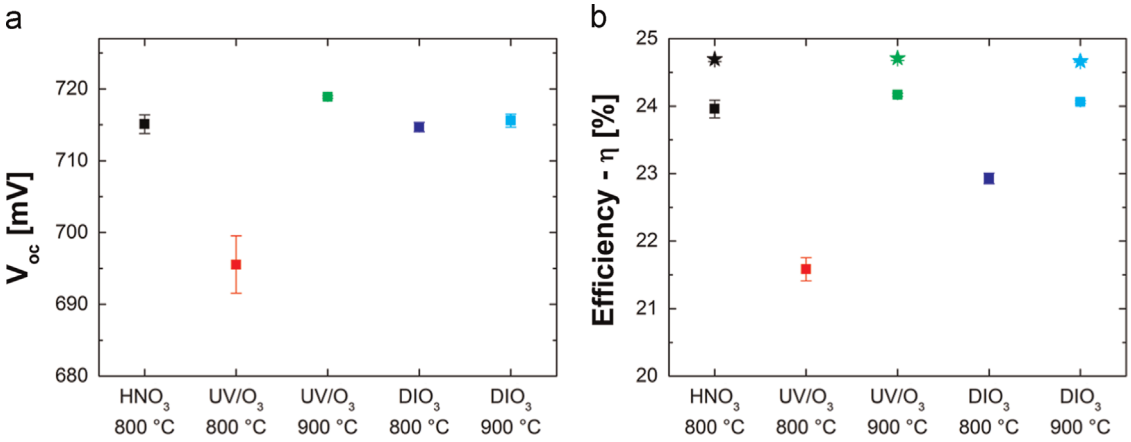


**Fig. 6.** (a) $V_{OC}$ values of the TOPCon solar cells. (b) Efficiency values of the TOPCon solar cells. The star symbols represent the efficiency values of the champion cells of each group.

passivation have been demonstrated. The recent findings of the XPS and TEM analysis give further evidence for the hypothesis that the stability of the passivation is dependent on the stoichiometry of the interfacial $SiO_x$ layer.

The different oxide layers were applied to solar cells featuring TOPCon as a full area passivated rear contact. High $V_{OC}$ values were reached for all investigated tunnel oxide layers. High efficiencies could be obtained especially for the $HNO_3$ reference process ($T_{anneal}$=800 °C) and for $UV/O_3$ and $DIO_3$ oxidation at $T_{anneal}$=900 °C. The variation in efficiency can be set in relation with the differences concerning the passivation properties at low injection conditions and the series resistance and is assumed to be coupled with the oxide properties.

## Acknowledgment

The authors would like to thank all co-workers at the Fraunhofer ISE; especially H. Brinckheger, A. Leimenstoll, F. Schätzle, S. Seitz, N. Weber and J. Wallner for sample preparation as well as E. Schäffer for measuring the solar cells. Thanks also apply to K. Kaufmann, V. Naumann and M. Werner from Fraunhofer CSP for XPS and TEM analysis. This work was supported by the German Federal Ministry for Economic Affairs and Energy within the research Projects under Contract number 0325292 “ForTes” and 0325634B “INNOHET”.

## References

[1] F. Feldmann, M. Bivour, C. Reichel, H. Steinkemper, M. Hermle, S.W. Glunz, Tunnel oxide passivated contacts as an alternative to partial rear contacts, Sol. Energy Mater. Sol. Cells 131 (2014) 46–50.
[2] F. Feldmann, M. Simon, M. Bivour, C. Reichel, M. Hermle, S.W. Glunz, Efficient carrier-selective p- and n-contacts for Si solar cells, Sol. Energy Mater. Sol. Cells 131 (2014) 100–104.
[3] A. Moldovan, F. Feldmann, G. Krugel, M. Zimmer, J. Rentsch, M. Hermle, A. Roth-Fölsch, K. Kaufmann, C. Hagendorf, Simple cleaning and conditioning of silicon surfaces with UV/ozone sources, Energy Procedia 55 (2014) 834–844.
[4] C.K. Fink, K. Nakamura, S. Ichimura, S.J. Jenkins, Silicon oxidation by ozone, J. Phys.: Condens. Matter 21 (2009) 183001.
[5] N. Awaji, S. Ohkubo, T. Nakanishi, Y. Sugita, K. Takasaki, S. Komiya, High-density layer at the $SiO_2$/Si interface observed by difference X-ray reflectivity, Jpn. J. App. Phys. 35 (1996) 67–70.
[6] N. Awaji, High-precision X-ray reflectivity study of ultrathin $SiO_2$ on Si, J. Vac. Sci. Technol. A 14 (1996) 971.
[7] Y. Sugita, S. Watanabe, N. Awaji, X-Ray reflectometry and infrared analysis of native oxides on Si (100) formed by chemical treatment, Jpn. J. Appl. Phys. 35 (1996) 5437–5443.
[8] U. Khalilov, G. Pourtois, A.C.T. van Duin, E.C. Neyts, On the c-Si\|a-$SiO_2$ interface in hyperthermal Si oxidation at room temperature, J. Phys. Chem. C 116 (2012) 21856–21863.
[9] W. Kern, D. Puotinen, Cleaning solutions based on hydrogen peroxide for use in silicon semiconductor technology, Rca Rev. 31 (1970) 187–205.
[10] H. Kobayashi, K. Imamura, W.-B. Kim, S.-S. Im, Asuha, Nitric acid oxidation of Si (NAOS) method for low temperature fabrication of $SiO_2$/Si and $SiO_2$/SiC structures, Appl. Surf. Sci. 256 (2010) 5744–5756.
[11] H. Kobayashi Asuha, O. Maida, M. Takahashi, H. Iwasa, Nitric acid oxidation of Si to form ultrathin silicon dioxide layers with a low leakage current density, J. Appl. Phys. 94 (2003) 7328.
[12] A. Fukano, H. Oyanagi, Highly insulating ultrathin $SiO_2$ film grown by photo-oxidation, J. Appl. Phys. 94 (2003) 3345.
[13] F. Feldmann, et al., Carrier-selective contacts for Si solar cells, in: Proceedings of the 40th IEEE PVSC, Denver, 2014.
[14] S. Lindekugel, H. Lautenschlager, T. Ruof, S. Reber, Plasma hydrogen passivation for crystalline silicon thin-films, in: Proceedings of the 23rd EUPVSEC, Valencia, 2008, pp. 2232–2235.
[15] M. Reusch, M. Bivour, M. Hermle, S.W. Glunz, Fill factor limitation of silicon heterojunction solar cells by junction recombination, Energy Procedia 38 (2013) 297–304.
[16] Y.J. Chabal, Fundamental Aspects of Silicon Oxidation, Springer-Verlag, Berlin, Heidelberg, New York, 2001.
[17] M. Hermle, et al., Approaching efficiencies above 25% with both sides-contacted silicon solar cells, in: Proceeding of the 42th IEEE PVSC, New Orleans, 2015.